Self-densified ultrathin solid electrolyte membrane fabricated from monodispersed sulfide electrolyte nanoparticles

Lilin Wu, Bai Xue, Hongjiao Wang, Zhenghua Su, Zhongkuan Luo, Fang Wang, Xianghua Zhang, Laurent Calvez, Bo Fan

To cite this version:

Lilin Wu, Bai Xue, Hongjiao Wang, Zhenghua Su, Zhongkuan Luo, et al.. Self-densified ultrathin solid electrolyte membrane fabricated from monodispersed sulfide electrolyte nanoparticles. Journal of the American Ceramic Society, 2022, 105 (12), pp.7344-7354. 10.1111/jace.18728 . hal-03797253

HAL Id: hal-03797253
https://hal.science/hal-03797253v1

Submitted on 11 Apr 2023

Self-densified ultrathin solid electrolyte membrane fabricated from monodispersed sulfide electrolyte nanoparticles

Lilin Wu [a,‡], Bai Xue [b,‡], Hongjiao Wang [b,c], Zhenghua Su [b], Zhongkuan Luo [a], Fang Wang [a], Xianghua Zhang [c], Laurent Calvez [c,*], Bo Fan [b,*]

a College of Chemistry and Environmental Engineering, Shenzhen University, Shenzhen 518060, China
b Shenzhen Key Laboratory of Advanced Thin Films and Applications, College of Physics and Optoelectronic Engineering, Shenzhen University, Shenzhen 518060, China
c Univ. Rennes, CNRS, ISCR (Institut des Sciences Chimiques de Rennes) UMR 6226, Rennes 35042, France

‡ These authors contributed equally to this work as co-first authors.

---

[*] Authors to be corresponded: fanb07@hotmail.com; laurent.calvez@univ-rennes1.fr.

Abstract:

Reducing particle size of sulfide electrolytes to nanoscale is essential for preparing ultrathin sulfide electrolyte membrane of all-solid-state batteries. However, there lacks effective way to synthesize sulfide electrolyte nanoparticles with good morphology uniformity. In this work, a dual precursor sol route is developed to speed up the synthesis of lithium thiophosphate from tens of hours by conventional liquid-phase routes to < 50 min. The promoted reaction kinetics inhibit the overgrowth of the product particles so that monodispersed lithium thiophosphate nanoparticles with sizes of 44±6 nm are prepared. Membranes fabricated from the nanoparticles achieve a thickness of 0.5–1.0 μm, which are reduced by one order of magnitude in comparison with those of reported sulfide electrolyte membranes. Moreover, the monodispersity makes the nanoparticles closely packed in the green membrane, so that the membrane can be self-densified without applying pressure, while 100-MPa-level pressure is indispensable for conventional membrane fabrication technologies. The ultrathin LPS membrane is also successfully employed in all-solid-state $LiFePO_4$ thin film batteries. This work not only provides a heuristic strategy to synthesis sulfide electrolyte nanoparticles, but also develops a pressing-free fabrication route of sulfide electrolyte membranes, which is eagerly demanded for high-energy-density all-solid-state batteries.

Key words: nanoparticles; sulfides; electrolyte; ionic conductivity; membranes; all-solid-state batteries.

1. Introduction

All-solid-state batteries have been considered as one of the candidates of next generation batteries because of their reliable safety and great potential of improving power density [1, 2]. To achieve the comparable energy density with conventional lithium-ion secondary batteries, all-solid-state batteries eagerly require solid electrolyte membranes with thicknesses < 30 μm.[3] Viewing the high ionic conductivity and the good mechanical properties of sulfide electrolytes,[4, 5] great efforts have been made to fabricate sulfide electrolyte membranes, including slurry process[6, 7] and dry-film process[8], which typically using binder[9] or scaffold[10, 11] to help shaping the membrane. Because the membranes are made from micron-sized sulfide electrolyte particles,[12, 13] the thickness of the membranes is limited to tens of microns.[10] Moreover, the irregular shape makes the particles cannot be closely packed. Therefore, a cold/hot-pressing process with a high pressure of 150–500 MPa is indispensable to densify the green membrane, which increases the process complexity for mass production. Recently, nano-sheets of sulfide electrolyte with lateral sizes of 1 μm and thicknesses of 80 nm are prepared by a newborn liquid-phase synthesis route.[14, 15] Benefiting of the reduced particle size, submicron sulfide electrolyte membranes are prepared from the nanosheets. To further improving the film-forming ability of the sulfide electrolyte particles, the morphology uniformity is another important factor, but has not been studied.

Rapid reaction kinetics, which favor burst nucleation and inhibit Ostwald ripening, are critical for synthesizing monodispersed nanoparticles.[16] Morphology uniformity of sulfide electrolyte particles at nanoscale should be achieved by identifying and accelerating the kinetics-limiting synthesis step. Here, the synthesis of Li_3PS_4 is studied, because it is a solid intermediate for most liquid-phase synthesized sulfide electrolytes, which controls the morphology of the final products.[17, 18] The reaction pathway for the formation of Li_3PS_4 includes two steps (Figure 1a). First, Li_2S and P_2S_5 rapidly react with a 1:1 molar ratio to form $Li_2S{\cdot}P_2S_5$ solution. Second, the excess Li_2S attacks the P-S-P bond in $Li_2S{\cdot}P_2S_5$ and Li_3PS_4 precursor (solvated by solvent molecular) precipitates.[19] Owing to the insolubility of Li_2S and Li_3PS_4, the second step, $Li_2S + Li_2S{\cdot}P_2S_5 \rightarrow Li_3PS_4$, is a sluggish solid-liquid reaction. Granular commercial Li_2S and P_2S_5 are usually used for liquid-phase synthesis. This even retards the second step, leading to the overgrowth and irregular shape of the products. Consequently, the Li_3PS_4 precursor appearing in conventional liquid-phase synthesis is always a suspension (Fig. 1b).

In this work, the kinetics-limiting reaction $Li_2S + Li_2S{\cdot}P_2S_5 \rightarrow Li_3PS_4$ is significantly accelerated by replacing the commercial powder of Li_2S and P_2S_5 with Li_2S sol and $Li_2S{\cdot}P_2S_5$ solution respectively, so that the overgrowth of the products is inhibited. Consequently, nanoparticles of lithium thiophosphate (LPS) are obtained for the first time, which possess excellent morphology uniformity and greatly reduced particle size (44±6 nm). Benefiting from the good film-forming ability of the monodispersed nanoparticles, uniform and compact submicron (0.5–1.0 μm) solid electrolyte membranes with resistances of 0.8 Ω cm^2 are prepared by simply spin coating. Remarkably, self-densification of the green membrane occurs without applying pressures. This work not only provides a heuristic strategy to synthesis nanoparticles of LPS and its derivatives, but also develops a pressing-free fabrication route for sulfide electrolyte membranes, which is practical for mass production of solid electrolyte membranes for high-energy-density all-solid-state batteries.

2. Experimental Section

2.1 Synthesis of materials

Li_3PS_4 precursor sol was synthesized by a dual precursor method. First, sulfur powder (99.5%, Alfa Aesar) and $LiEt_3BH$ solution in tetrahydrofuran (THF, 1 M, Innochem) were used as the starting materials to prepare Li_2S sol with a concentration of 1M. The as-prepared Li_2S was centrifugated and re-dispersed in THF (≥99.5%, Aladdin). Then, 322-mg of a mixture of commercial Li_2S (99.9%, Alfa Aesar) and P_2S_5 (99.9%, Aladdin) with a molar ratio of 1:1 was dispersed in 15 mL acetonitrile (ACN, ≥99.5%, Aladdin). A light yellow $Li_2S \cdot P_2S_5$ solution was obtained after 30-min stirring. Finally, the Li_2S sol and $Li_2S \cdot P_2S_5$ solution were mixed to obtain a colorless and transparent Li_3PS_4 precursor sol, in which totally the molar ratio of Li_2S and P_2S_5 was 3:1. The precursor sol was dried at 60°C and subsequently heat-treated at 250°C under argon for 1h to obtain the LPS solid electrolytes. For comparison, β-Li_3PS_4 was also prepared by conventional suspension method. Commercial powders of Li_2S and P_2S_5 at a molar ratio of 3:1 were mixed in ACN. The mixture was stirred for 3 days. The resultant precursor suspension was dried and heat-treated in the same way as above. The nano-Li_2S was also applied in conventional route, that is, mixed with the P_2S_5 powder in a mixed solvent (THF: ACN=2:1) to prepare the LPS solid electrolyte.

Considering the high price of the $LiEt_3BH$ solution, an alternative route by replacing the $LiEt_3BH$ solution with a Li-naphthalene (Naph) solution was also studied. The Li_2S sol could also be prepared by mixing Li-Naph solution and sulfur powder. First, naphthalene and lithium chips were dispersed in 1,2-dimethoxyethane (DME) to prepare 0.5 M Li-Naph solution, into which the sulfur powder was then added and stirred for 3 h to synthesize Li_2S nanoparticles. Then, the as-prepared Li_2S nanoparticles were centrifugated and re-dispersed in THF. The obtained Li_2S sol was used to react with the $Li_2S \cdot P_2S_5$ solution so that the Li_3PS_4 precursor sol could be prepared as described above. Considering the sensitivity of the materials to moisture and oxygen, all the operations were conducted in an argon-filled glovebox ($H_2O<0.5$ ppm, $O_2<0.5$ ppm).

2.2 Characterization of materials

The X-ray diffraction patterns of the powder samples were collected on a Bruker D8 Advance X-ray diffractometer with a Cu K_α radiation source. Diffraction data was collected in the 2θ range from 10° to 60°. Raman spectroscopy was performed using a Raman spectrometer (inVia, Renishaw Inc., UK) equipped with a green laser (532 nm). The laser power was 5% and a 50X objective was used. Samples for XRD and Raman measurements were prepared in glovebox on glass slides and sealed with polyimide film. All the XRD patterns show two broad peaks around 12° and 20°, which were attributed to the polyimide film. Morphology of the samples was observed by a field-emission scanning electron microscope (Zeiss Supra 55, Carl Zeiss GmbH, Germany). Samples were transferred from the glovebox to SEM through a vacuum sample holder. The ionic conductivity of materials was examined by AC impedance spectroscopy using an impedance analyzer (Solartron1260A, Solartron Analytical Inc., UK) in the frequency range of 1.0 MHz–0.1 Hz. The amplitude of the AC voltage was 15 mV. For the impedance measurement, the solid electrolyte powder (about 200 mg) was cold-pressed into disks (φ 15 mm) under 360 MPa pressure. Gold film was then deposited by a low vacuum coater (EM ACE200, Leica Microsystems, Germany) on the both sides of the disks as the inert electrodes.

2.3 Fabrication of LPS solid electrolyte membranes

Submicron LPS membranes were fabricated using Li_3PS_4 precursor sol via spin coating technique. Glass sheets covered with gold film were used as the substrates for spin coating. The glass substrates were ultrasonically cleaned in detergent (1% in water), anhydrous ethanol and deionized water in sequence, and dried with N_2 flow. Then gold film was deposited on the glass substate with a low vacuum coater (EM ACE200, Leica Microsystems, Germany). The concentration of the LPS sol was adjusted to be 0.13 M for spin coating. The spin coating was conducted at 4000 rpm. The free solvent rapidly evaporated, resulting in a transparent membrane. The membrane was then transferred onto a hotplate preset at 250°C to remove the solvated organic molecules. The thickness of the membrane could be increased by repeating the above operations. Finally, the membranes were sintered at 250°C under vacuum for 1 h. The spin coating was operated in a glovebox.

2.4 Assembling of $LiFePO_4$ thin film battery

The $LiFePO_4$ cathode was prepared by mixing $LiFePO_4$ powder, KB, PVDF binder, PEO, and bistrifluoromethanesulfonimide lithium salt (LiTFSI) with a weight ratio of 6:1:1:1:1 in N-methylpyrrolidone (NMP). The resulting slurry was casted on a carbon-coated aluminum foil with a doctor blade and dried at 80°C for 24 h under vacuum. The mass loading of the active material was ~ 0.5 mg cm^{-2}.

A LPS membrane with a thickness of 860 nm was spin-coated on an Au/glass substrate, with a corner of the Au film exposed as a bottom electrode. To attach the cathode to the LPS membrane, the surface of the cathode was covered with a sticky layer of polyethylene oxide (PEO) electrolyte by spin-coating. The PEO electrolyte was prepared by dissolving 0.3 g PEO and LiTFSI (EO:Li^+=18:1) in 10 mL ACN. Then, the $LiFePO_4$ cathode was pressed on the LPS membrane at 80°C. The freshly assembled $LiFePO_4$ battery was conducted to electroplate lithium on Au film at 60°C at a current of 25 μA cm^{-2} with a capacity of 37.5 μAh cm^{-2}, and the obtained Li-Au alloy was used as anode of the $LiFePO_4$ thin film battery.

3. Results and discussion

3.1 Monodispersed sulfide electrolyte nanoparticles

Inspired by the two-step reaction mechanism of the conventional liquid-phase synthesis of LPS, we design a dual precursor route to improve the morphology control of the products by promoting the reaction kinetics. As shown in Fig. 1c. The route starts with the preparation of two precursors, a sol containing nano-Li_2S and a solution containing $Li_2S{\cdot}P_2S_5$. Here the Li_2S sol is synthesized by the reaction between S and $LiEt_3BH$. The two precursors replace commercial powders of Li_2S and P_2S_5 respectively. Then they are mixed to react. The large specific area of Li_2S nanoparticles and the wettability of $Li_2S{\cdot}P_2S_5$ solution significantly promote the reaction kinetics so that overgrowth of the product is greatly inhibited. Finally, solvated Li_3PS_4 nanoparticles are obtained. The transparent LPS precursor sol shows obvious Tyndall effect (a typical scattering phenomenon of sol) under the illumination of a green laser

(Fig. 1d), which is in sharp contrast with the turbid LPS suspension by conventional route (Fig. 1b).

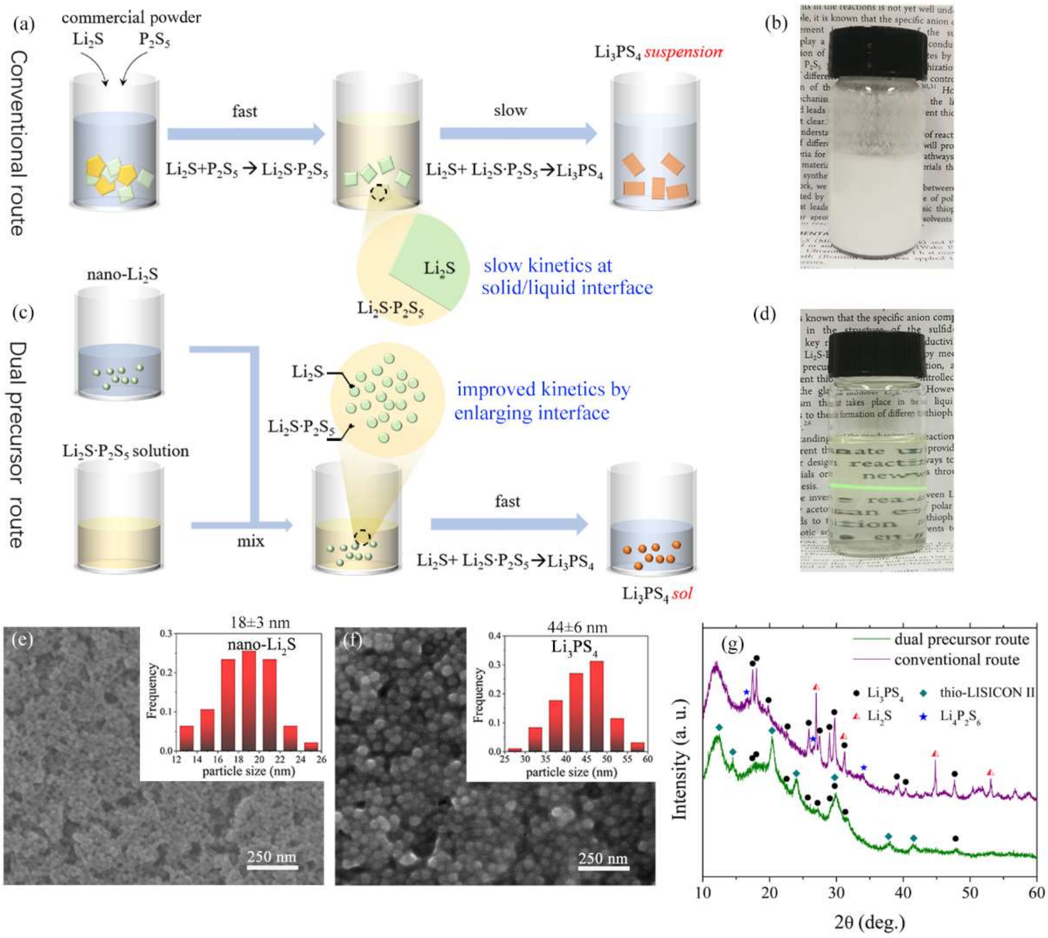

Figure 1 (a) Two-step reaction mechanism of conventional suspension route of LPS. The sluggish kinetics of the second step reaction lead to overgrowth and poor morphology uniformity of LPS precursor. (b) Photo of LPS suspension prepared by conventional route. (c) Schematic of dual precursor route which exhibit excellent morphology control of LPS precursor by improving the reaction kinetics. (d) Photo of LPS sol prepared by dual precursor route. Tyndall effect of the sol is demonstrated. SEM images and size distribution of (e) nano-Li_2S and (f) resultant LPS precursor particles. (g) XRD patterns of LPS prepared by conventional route and dual precursor route.

The nanoscale size distribution of the LPS particles prepared by dual precursor route is unambiguously verified by SEM. The nano-Li_2S is of good size uniformity and the size is 18±3 nm (Fig. 1e), corresponding to the broadening of XRD and Raman signals (Fig. S1). These monodispersed nano-Li_2S particles not only provide large amounts of solid/liquid interface to accelerate the react with $Li_2S{\cdot}P_2S_5$, but also create uniform additional driving force for the reaction by their spherical surfaces with monodispersed curvatures. Consequently, nanoparticles of LPS precursor with average sizes of 44 nm and a small standard deviation of 6 nm are prepared (Fig. 1f). It is worth noting that these LPS particles show a uniform spherical morphology, different from those prepared by suspension route, which show prismatic shape with large size of ~10 μm or irregular nanosheets with lateral sizes of ~1 μm.[15, 20]

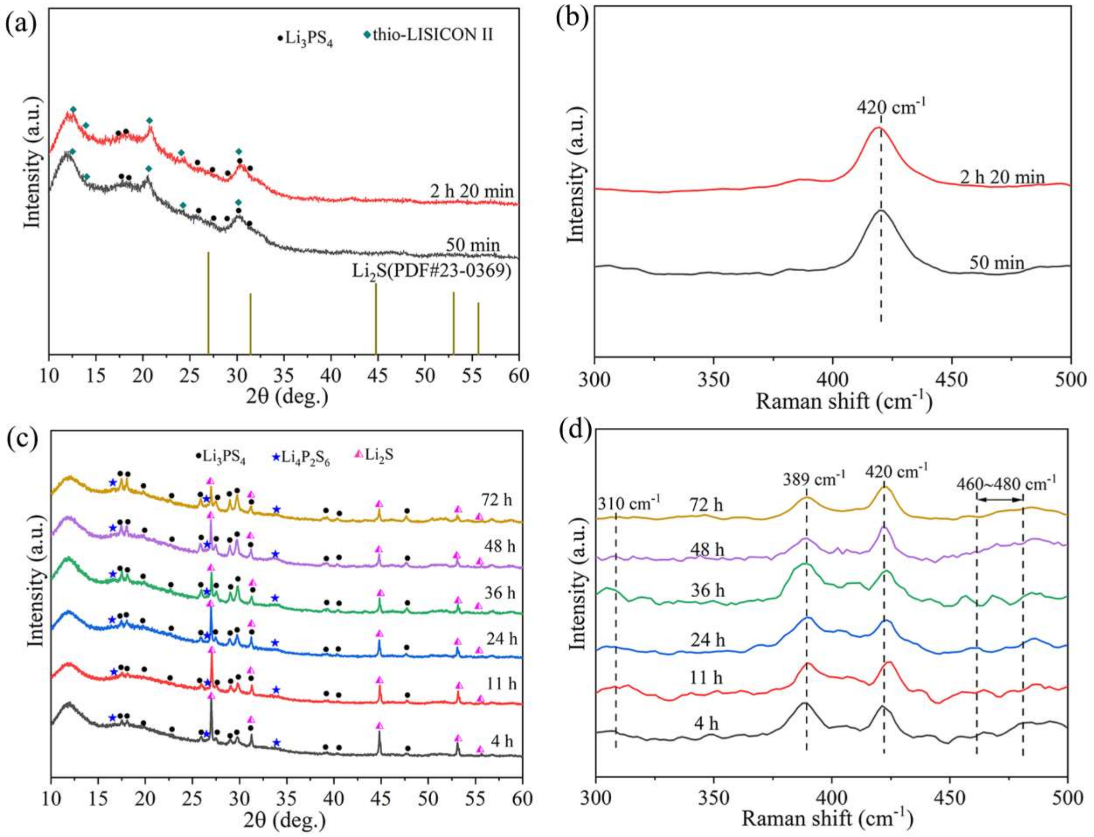

Figure 2 Comparison of the reaction rate by dual precursor route and by conventional suspension route.

(a) XRD patterns and (b) Raman spectra of the solid electrolyte prepared by dual precursor route with different reaction durations. (c) XRD patterns and (d) Raman spectra of the solid electrolyte prepared by conventional suspension route with different reaction durations. Impurities Li_2S and $Li_4P_2S_6$ are absent in the solid electrolyte prepared by dual precursor route.

LPS precursor containing solvated solvent molecules. XRD results identify that its principal phase is $Li_3PS_4{\cdot}ACN$ (Fig. S2a). After heat treatment at 250°C, the solvent is removed (Fig. S2b and Fig. S3). The obtained sulfide electrolyte contains β-Li_3PS_4 and thio-LISICON II, and is free of poorly conductive impurities such as Li_2S and $Li_4P_2S_6$ (Fig. 1g). β-Li_3PS_4 and thio-LISICON II are room-temperature metastable phase with high ionic conductivities, which are initially discovered in Li_2S-P_2S_5 glass-ceramics with Li_2S content higher than 75 mol.%.[21, 22] The room-temperature conductivity of the obtained sulfide electrolyte is 3.87×10^{-5} S cm^{-1}(Fig. S4). This value is somehow lower than that prepared by conventional suspension routes,[20, 23] which may be caused by the residual by-products such as Et_3B. Kaup et al. proposed that, when Li_3PS_4 is prepared by liquid phase method, to completely remove the residual solvent and decomposition products, the annealing temperature should be above 400°C, but the nanostructure could be destroyed.[24] Thus, we try a moderately higher heat-treatment temperature of 300°C to obtain purer Li_3PS_4, and achieve higher conductivity of 1.69×10^{-4} S cm^{-1} (Fig. S5), which is comparable to that prepared by conventional liquid-phase synthesis.

Viewing the importance of the kinetics of the reaction $Li_2S + Li_2S{\cdot}P_2S_5 \rightarrow Li_3PS_4$ for morphology control during liquid-phase synthesis, how fast this reaction is promoted by dual precursor route is examined. It is done by monitoring the phase evolution of the solid electrolytes with different reaction time. The reaction time is recorded since the $Li_2S{\cdot}P_2S_5$ solution and Li_2S sol are mixed, until the obtained dual precursor sol is dried completely under an argon flow. To avoid the acceleration of the reaction by heating, the drying is conducted at room temperature. Thus, the minimal reaction time, which is achieved by directly starting the drying after the raw material mixing, is 50 min. The solid electrolytes with reaction duration of 50 min and 2 h 20 min present identical XRD patterns (Fig. 2a), both containing β-Li_3PS_4 and a small amount of thio-LISICON II, while the signals of the raw material Li_2S completely disappear. Correspondingly, except the Raman band attributing to the symmetric stretching of P-S bonds in PS_4^{3-} (420 cm^{-1}),[25] which constitutes β-Li_3PS_4 and thio-LISICON II,[22] signals belonging to other structure units are hardly detected for all reaction durations (Fig. 2b). It is therefore concluded that the reaction of dual precursor route is completed within 50 min. For comparison, LPS suspension is prepared with conventional liquid-phase synthesis, by directly mixing commercial Li_2S and P_2S_5 in ACN. As shown by the XRD results, the signals of Li_2S weaken and the signals of β-Li_3PS_4 intensify after a long-time reaction (Fig. 2c). However, Li_2S is still observed after 72-h reaction, indicating that the reaction is not completed.

Remarkably, the promoted reaction kinetics not only provide better morphology control of the products, but also eliminate the impurities. During conventional suspension route, the unreacted $Li_2S{\cdot}P_2S_5$ turns into $Li_4P_2S_6$ after heat treatment,[17] as shown by the X-ray diffraction peaks and characteristic Raman bands (Fig. 2c-d). The obvious band at 389 cm^{-1} attributes to the stretching of P-S bonds in PS_3 terminal modes of $P_2S_6^{4-}$.[26] The weak peak at 310 cm^{-1} can be attributed to the stretching of P-P and the bending of S-P-S in $P_2S_6^{2-}$, and the peak between 460 cm^{-1} and 480 cm^{-1} is the signal of the stretching of P-S bonds in $P_2S_6^{2-}$.[27]

The LPS is also synthesized by mixing the P_2S_5 powder with the nano-Li_2S in a mixed solvent (THF: ACN=2:1). Similar reaction time of 65 min with the dual precursor route is chosen, and 1 h heat treatment at 250°C under argon is subsequently applied. As shown by the XRD results (Fig. S6), besides β-Li_3PS_4 and thio-LISICON II, the signal of Li_2S can still be observed in the product. These results confirm that, preparing the $Li_2S \cdot P_2S_5$ solution in advance is very crucial to promote the reaction homogeneity and eliminate the residual raw materials. The thorough reaction between Li_2S and $Li_2S \cdot P_2S_5$ by dual precursor route eliminates these poorly conductive impurities (Fig. 2a-b), benefiting the ionic conductivity of the solid electrolyte.

Using the reaction between $LiEt_3BH$ and S to prepare nano-Li_2S greatly increases the cost of the dual precursor sol route. Fortunately, there are many other inexpensive synthetic methods of nano-Li_2S.[28-30] As an example, here it is demonstrated that by using the nano-Li_2S prepared by an inexpensive way, that is, mixing sulfur powder and Li-Naph solution,[31] the LPS nanoparticles can also be successfully synthesized by the dual precursor sol method (Fig. S7). Similarly, after heat treatment at 250°C, sulfide electrolyte containing β-Li_3PS_4 and thio-LISICON II is obtained (Fig. S8), and its ionic conductivity at room temperature is 2.8×10^{-5} S cm^{-1} (Fig. S9). This demonstrates the high flexibility of the dual precursor sol route for the synthesis of LPS nanoparticles, which benefits the modification of the synthesis route for satisfying the requirements for specific applications.

3.2 Self-densified submicron sulfide electrolyte membrane

Compared with the conventional synthesis technologies of sulfide electrolytes, the novel dual precursor route significantly reduces the particle size to nanoscale and improves the morphology uniformity. These features endow the nanoparticles with distinguished film-forming ability (Fig. 3a). First, the nanoparticles provide large amounts of highly active surface. Combined with the high Li diffusivity of sulfide electrolytes which facilitates low-temperature sintering,[32] the nanoparticles exhibit excellent sinterability. Second, the good morphology uniformity makes the nanoparticles closely packed, reduces the porosity of the green membranes (Fig. 1f). Consequently, the ultrathin solid electrolyte membrane can be fabricated by spin-coating of the precursor sol. Even though a high sintering temperature of 300°C greatly improves the ionic conductivity of LPS, it causes serious thermal stress in the membrane. Therefore, the green membrane is sintered at lower temperature of 250°C. Despite the conductivity of the 250°C-sintered LPS is lower, it is sufficient for fast ion conduction in a submicron solid electrolyte membrane as shown below. It is worth noting that no pressing is needed here, while it is an indispensable step to densify sulfide electrolyte membranes by other reported technologies.

Fig. 3b shows the digital picture and SEM image of the LPS membrane prepared from the sulfide electrolyte nanoparticles. The picture shows a transparent LPS membrane on gold film. In the SEM image, it can be seen that the surface of LPS membrane is dense and uniform, without any micropores and cracks. There is an obvious sintering phenomenon among LPS particles in comparison with the green membrane (Fig. 1f). The cross-sectional SEM image (Fig. 3c) shows that the thickness of the LPS membrane is about 550 nm. This also shows the compact structure over the whole membrane.

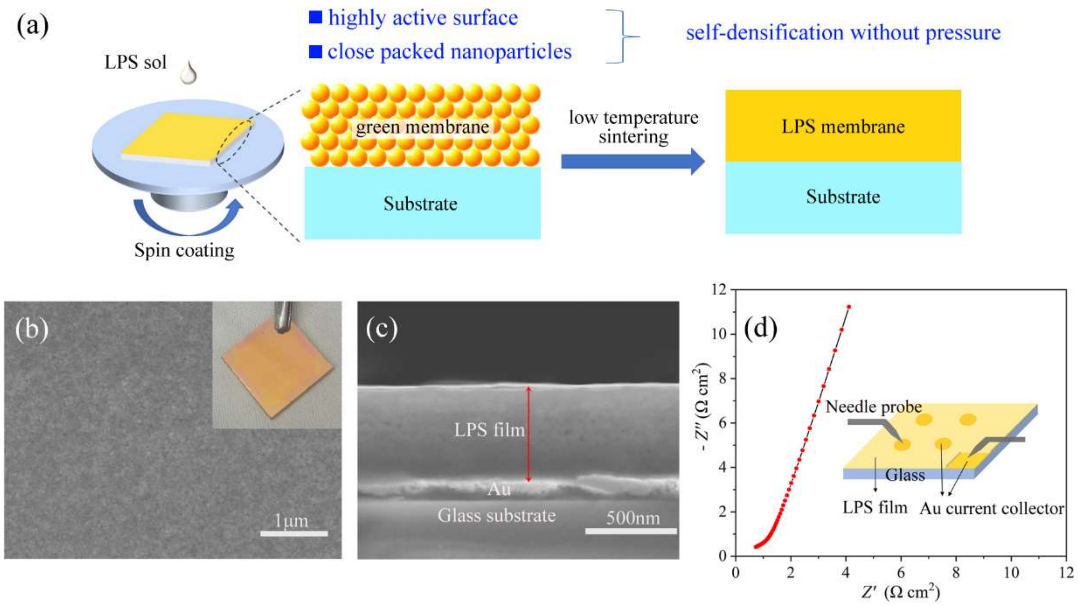

Figure 3 (a) Schematic of the fabrication of self-densified ultrathin LPS membrane from the precursor sol containing LPS nanoparticles. (b) Top-view and (c) cross-sectional SEM images of a LPS membrane with a thickness of 550 nm after low-temperature sintering at 250°C. The insert shows a transparent LPS film on gold film. (d) Nyquist plot of the LPS membrane. A schematic of the setup for the impedance spectroscopy measurement is illustrated in the insert.

To characterize the ion conduction ability of the LPS membrane, the membrane is fabricated on gold-film-coated glass substrates by spin coating. After sintering, gold disks are further deposited on the membrane as top electrodes for the impedance spectroscopy measurement. Fig. 3d is the Nyquist plot of the LPS film. Owing to the high-frequency limit of the measurement system, the impedance spectroscopy does not show a complete semicircle corresponding to the resistance of the film, and presents only an oblique line attributed to the polarization near the electrodes. It can be seen that the intersection of the oblique line and the Z' axis is 0.8 Ω cm^2. It represents the specific resistance of the LPS film which is much smaller than that of the thick membranes fabricated by cold pressing.[33, 34] Remarkably, the ionic conductivity of the membrane is calculated to be 6.7×10^{-5} S cm^{-1}. This value is even higher than 3.87×10^{-5} S cm^{-1}, which is measured from the impedance spectra of the cold-pressed LPS pellet. It implies that the self-densification of the LPS nanoparticles by low temperature sintering is more effective than that by cold-pressing, a conventional densifying approach for sulfide electrolytes.[35]

3.3 Performance of the sulfide electrolyte membrane

The characteristics of typical reported sulfide electrolyte membranes are compared (Fig. 4a and Tab. S1). It can be seen that the membrane prepared by the LPS nanoparticles exhibits a low resistance approaching the state-of-the-art value, while its thickness is reduced by one order of magnitude. More importantly, no pressure is needed to densify the membrane, simplifying the membrane fabrication process. To demonstrate how the ultrathin LPS membrane benefits the energy density of the battery, the energy density of an all-solid-state lithium-sulfur battery using a LPS membrane is estimated following the approach described in Ref. 5. The parameters for the estimation are listed in Tab. S2. As shown in Fig. 4b, when using a 1-μm thick membrane, only a low cathode loading of 1.7 mg cm^{-2} is required to achieve a practical energy density of 400 W h kg^{-1}. To achieve this energy density level, the cathode loading should be increased to 5 mg cm^{-2} when using a 30-μm thick membrane. Increasing cathode loading is accompanied with a series of issues, such as deteriorated electrical conduction in the cathode, mechanical collapse of the composite structure owing to large volumetric fluctuation of active materials and a high current density which induces additional problems at the lithium anode side.[36] A combination of a ultrathin solid electrolyte membrane and a relative low active material loading could be a facile way to achieve practical energy density of all-solid-state batteries.

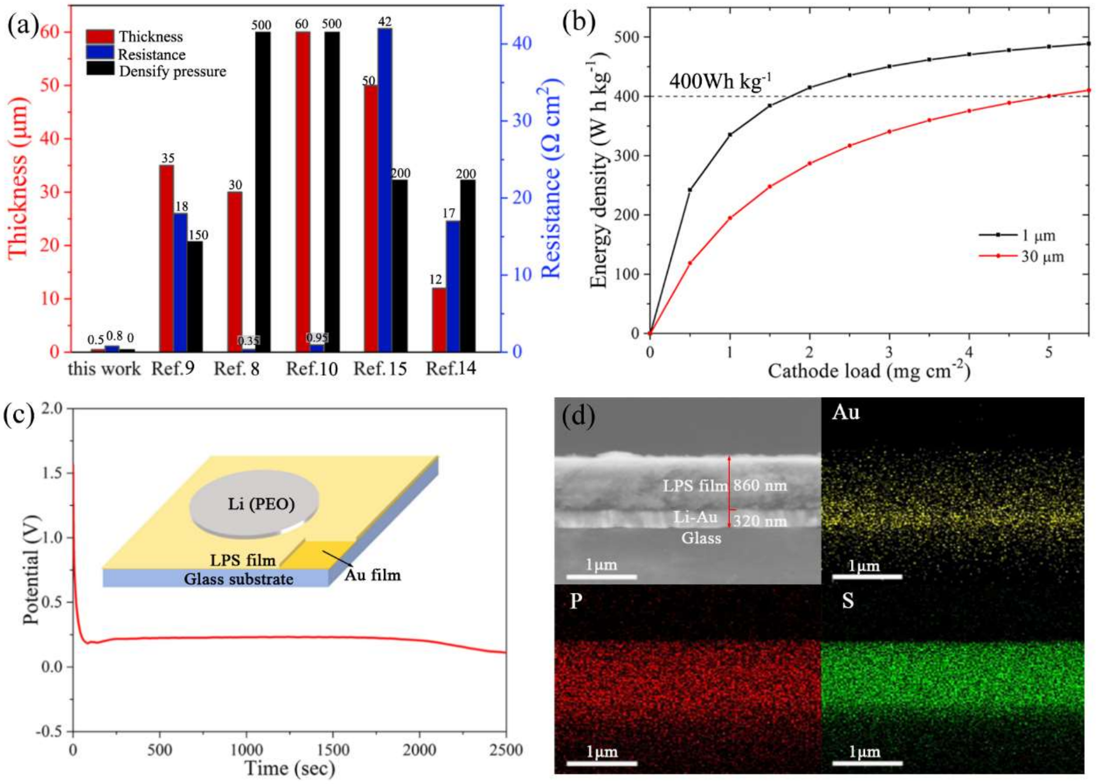

Figure 4 (a) Thickness, resistance and densify pressure of reported sulfide electrolyte membranes. Unit for densify pressure is MPa. (b) Estimation of the energy density of all-solid-state Li-sulfur batteries using 1-μm thick and 10-μm thick LPS membranes. (c) Chronopotentiometric profile of Li plating with a +) Au/LPS membrane/Li (− half-cell. A schematic of the cell structure is illustrated in the insert. (d) SEM image and EDS elemental mapping of the cross section of the half-cell after lithium deposition with a capacity of 46.3 μAh cm^{-2} at a current of 65 μA cm^{-2}.

To demonstrate the electrochemical performance of the ultrathin LPS membrane, a +) Au /LPS membrane/ Li (− half-cell is assembled and lithium deposition behavior is tested. The schematic of the cell structure is illustrated in Fig. 4c. First, a LPS membrane with a thickness of 860 nm (Fig. 4d) is spin-coated on an Au/glass substrate, with a corner of the Au film exposed as a bottom electrode. Then, a lithium foil spin-coated with a thin layer of PEO electrolyte is pressed on the LPS membrane at 80°C, so that the half-cell is assembled. To prepared the PEO-coated lithium foil, 0.030 g PEO and 0.012 g LiTFSI ($EO:Li^+=18:1$) is firstly dissolved in 10 mL 1,3-dioxolane (DOL), and then 100 μL solution is spin-coated on the lithium foiled and left drying at room temperature to remove the solvent. The lithium deposition test is conducted with a current of 65 $\mu A\ cm^{-2}$ at 60°C. Generally, the lithium deposition includes alloying and lithium dendrite growth stages.[37, 38] Firstly, Au is slowly lithiated and Li_2Au alloy is formed. Then, with the continuous deposition of lithium, Li_2Au is transformed into Li_3Au. When the lithium in Li-Au alloy reaches saturation, lithium dendrite tends to grow. These processes correspond to three voltage platforms respectively. It can be seen from the voltage profile (Fig. 4c), once lithium deposition begins, the voltage drops sharply. Then, the voltage gradually stabilizes at 0.23 V, which represents that Au is gradually lithiated and Li_2Au alloy forms. Then the second platform at 0.10 V(~ 2000-2500 s) emerges which is associated with the formation of Li_3Au alloy. The total deposition capacity is 46.3 $\mu Ah\ cm^{-2}$. The excellent lithium deposition stability benefits from the great densification and uniformity of the LPS membrane.

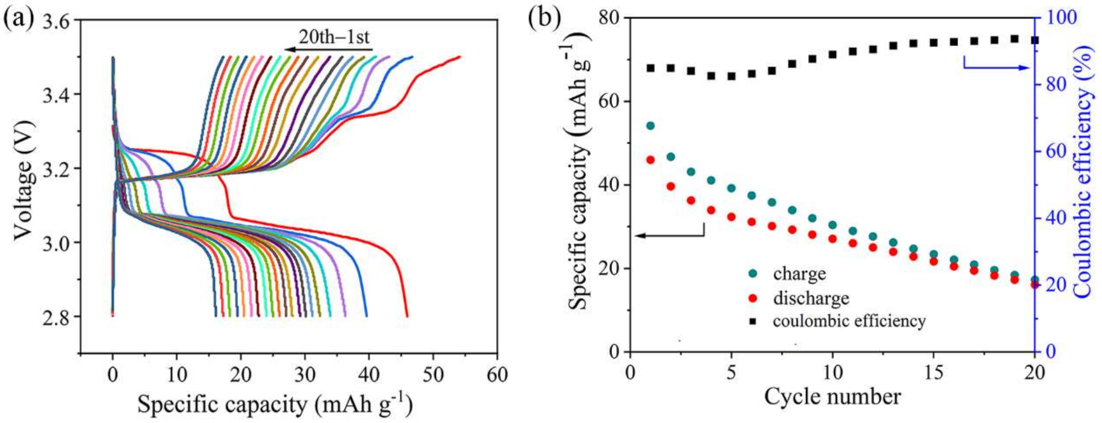

Figure 5 (a) The galvanostatic charge/discharge curve and (b) Cycling performance at a current of 25 μA cm^{-2} of all-solid-state $LiFePO_4$ thin film battery.

As can be seen from the cross-sectional SEM image in Fig. 4d, the thickness of Au film increases significantly after lithium deposition, from initial 85 nm (Fig. S10) to 320 nm. The EDS mapping and line scanning results (Fig. S11) show that the signal of Au weakens and spreads, which is consistent with the formation of Li-Au alloy during lithium deposition. Additionally, element analysis (Fig. 4d and S11) reveals the diffusion of elements P and S into the deposited metal layer, which is a direct manifestation of the reaction between LPS and Li. Theoretical and experimental studies clarify that the reaction of sulfide electrolytes with lithium metal can be driven by thermodynamic factors and generates Li_3P, Li_2S and other decomposition products, which constitute solid-electrolyte interphase (SEI) layer.[39-41] It is worth noting that evident migration of P and S into the deposited metal layer occurs within only 2500 s, indicating a rapid reaction occurs concomitantly with the lithium deposition. It implies the intimate contact between the bottom electrode and the spin-coated LPS membrane since good contact promotes interfacial reaction rate.[42]

The ultrathin LPS membrane is further applied to all-solid-state $LiFePO_4$ thin film batteries. As shown in Fig. 5, two discharge platforms are observed at 3.24 V and 3.05 V. The equilibrium potential of $LiFePO_4$ is 3.42 V vs. Li/Li^+.[43] Considering the fact that the potential of Li_3Au and Li_2Au are about 0.10 and 0.23 V vs. Li/Li^+ (Fig. 4c), and considering also the overpotential during discharge of the battery, it can be concluded that the two discharge platforms correspond to the potential platforms of Li_3Au and Li_2Au, respectively. The initial discharge capacity is 45.9 mAh g^{-1}. It becomes 16.1 mAh g^{-1} after 20 cycles. Meanwhile, the coulombic efficiency increases from 84.9% to 93.2%. The low capacity may be ascribed to the consumption of Li by the reaction with LPS, which is supported by the low initial coulombic efficiency. The consumption of Li also hinders the transition from Li_2Au to Li_3Au, leading to the gradually disappearance of the discharge platform at 3.24 V. This problem is expected to be solved by using Li electrode with an excess amount of Li instead of the Au electrode. This requires a modified LPS precursor sol compatible with lithium, which is under development in our laboratory. Whatever, the operation of the $LiFePO_4$ thin film battery proves that the membrane prepared by LPS nanoparticles is of great potential to develop all-solid-state batteries.

Remarkably, reducing the particle size of sulfide electrolytes into nanoscale not only provides opportunities for the preparation of self-densified ultrathin membranes, but also potentially opens up a new way towards many applications. For example, studies show that reducing particle size of solid electrolytes in composite solid cathode can improve the electrode-electrolyte contact and augment cathode loading.[44, 45] Therefore, this new technology of nano-LPS electrolyte is of great potential to be used for nano-composite cathodes. In addition, porous structure can be easily fabricated from the sol, so that the sol-synthesis route can be further developed to prepare nano-porous sulfide solid electrolytes. The porous structure has been demonstrated having excellent anti-lithium-penetration ability for all-solid-state lithium metal batteries.[46]

4. Conclusion

In summary, the sluggish kinetics of a universal reaction, $Li_2S+Li_2S{\cdot}P_2S_5 \rightarrow Li_3PS_4$, result in overgrowth and poor morphology controllability of liquid-phase synthesized sulfide electrolytes. By replacing the commercial powder of Li_2S and P_2S_5 with Li_2S sol and $Li_2S{\cdot}P_2S_5$ solution, this basic reaction is significantly accelerated to less than 50 min. Consequently, monodispersed Li_3PS_4 nanoparticles with size of 44±6 nm are prepared for the first time, which are then used to construct self-densified ultrathin solid electrolyte membranes. Benefiting from the excellent film-forming ability of the monodispersed nanoparticles, ultrathin solid electrolyte membranes with a thickness of ~550 nm are fabricated by spin coating. The as-prepared membranes can be simply densified after sintering at low temperature of 250°C, without applying any pressure. The membranes possess remarkably small specific resistance of $0.8\ \Omega\ cm^2$ and stable lithium deposition performance at $65\ \mu A\ cm^{-2}$. Besides, the LPS membrane is successfully employed in all-solid-state $LiFePO_4$ batteries. The dual precursor sol method opens new path toward the nano-sized sulfide electrolytes, and provides an effective strategy of preparing ultrathin sulfide solid electrolyte membranes for high energy density all-solid-state batteries.

Conflict of Interest

The authors declare that they have no known competing financial interests or personal relationships that could have appeared to influence the work reported in this paper.

Supporting Information.

Supporting Information is available online.

Contribution Statement

Lilin Wu： Investigation, Writing-Original Draft. **Bai Xue**: Conceptualization, Methodology. **Hongjiao Wang**: Investigation, Validation. **Zhenghua Su**: Methodology. **Zhongkuan Luo**: Supervision, Writing-Review & Editing. **Fang Wang**: Resource, Funding acquisition. **Xianghua Zhang**: Resource, Writing-Review & Editing. **Laurent Calvez**: Supervision, Funding acquisition, Writing-Review & Editing. **Bo Fan**: Supervision, Conceptualization, Funding acquisition.

Acknowledgements

The work is financially supported by the Natural Science Foundation of Guangdong Province (2021A1515011725), the Stable Support Plan for Shenzhen Higher Education Institutions (20200811211215001) and the Shenzhen Science and Technology Foundation (20210312150925001).

References

1. B. Ding, J. Wang, Z. Fan, S. Chen, Q. Lin, X. Lu, et al. Solid-state lithium–sulfur batteries: Advances, challenges and perspectives. Mater Today. 2020; 40: 114-131.
2. J. Schnell, T. Günther, T. Knoche, C. Vieider, L. Köhler, A. Just, et al. All-solid-state lithium-ion and lithium metal batteries – paving the way to large-scale production. J Power Sources. 2018; 382: 160-175.
3. C. Li, H. Zhang, L. Otaegui, G. Singh, M. Armand, L. M, et al. Rodriguez-Martinez Estimation of energy density of Li-S batteries with liquid and solid electrolytes. J Power Sources. 2016; 326:1-5.
4. Y. Kato, S. Hori, T. Saito, K. Suzuki, M. Hirayama, A. Mitsui, et al. High-power all-solid-state batteries using sulfide superionic conductors. Nat Energy. 2016; 1:16030.
5. Y. Zhang, R. Chen, T. Liu, Y. Shen, Y. Lin, C. W. Nan, et al. High Capacity, Superior Cyclic Performances in All-Solid-State Lithium-Ion Batteries Based on $78Li_2S$-$22P_2S_5$ Glass-Ceramic Electrolytes Prepared via Simple Heat Treatment. ACS Appl Mater Interfaces. 2017; 9: 28542-28548.
6. Y.-G. Lee, S. Fujiki, C. Jung, N. Suzuki, N. Yashiro, R. Omoda, et al. High-energy long-cycling all-solid-state lithium metal batteries enabled by silver–carbon composite anodes. Nat Energy. 2020; 5:299-308.
7. Y. J. Nam, S.-J. Cho, D. Y. Oh, J.-M. Lim, S. Y. Kim, J. H. Song, et al. Bendable and Thin Sulfide Solid Electrolyte Film: A New Electrolyte Opportunity for Free-Standing and Stackable High-Energy All-Solid-State Lithium-Ion Batteries. Nano Lett. 2015; 15: 3317-3323.

8. Z. Zhang, L. Wu, D. Zhou, W. Weng, X. Yao, et al. Flexible Sulfide Electrolyte Thin Membrane with Ultrahigh Ionic Conductivity for All-Solid-State Lithium Batteries. Nano Lett. 2021; 21: 5233-5239.
9. G. Liu, J. Shi, M. Zhu, W. Weng, L. Shen, J. Yang, et al. Ultra-thin free-standing sulfide solid electrolyte film for cell-level high energy density all-solid-state lithium batteries. Energy Stor Mater. 2021; 38: 249-254.
10. G.-L. Zhu, C.-Z. Zhao, H.-J. Peng, H. Yuan, et al. A Self-Limited Free-Standing Sulfide Electrolyte Thin Film for All-Solid-State Lithium Metal Batteries. Adv Funct Mater. 2021; 31: 2101985.
11. R. Xu, J. Yue, S. Liu, J. Tu, F. Han, P. Liu, et al. Cathode-Supported All-Solid-State Lithium–Sulfur Batteries with High Cell-Level Energy Density. ACS Energy Lett. 2019; 4:1073-1079.
12. J. Kim, Y. Yoon, J. Lee, D. Shin , et al. Formation of the high lithium ion conducting phase from mechanically milled amorphous $Li_2S–P_2S_5$ system. J Power Sources. 2011; 196: 6920-6923.
13. K. Minami, F. Mizuno, A. Hayashi, M. Tatsumisago, et al. Lithium ion conductivity of the $Li_2S–P_2S_5$ glass-based electrolytes prepared by the melt quenching method. Solid State Ionics. 2007; 178:837-841.
14. Z. D. Hood, H. Wang, A. S. Pandian, R. Peng, K. D. Gilroy, M. Chi, et al. Fabrication of Sub-Micrometer-Thick Solid Electrolyte Membranes of β-Li_3PS_4 via Tiled Assembly of Nanoscale, Plate-Like Building Blocks. Adv Energy Mater. 2018; 8: 1800014.

15. H. Wang, Z. D. Hood, Y. Xia, C. Liang, et al. Fabrication of ultrathin solid electrolyte membranes of β-Li_3PS_4 nanoflakes by evaporation-induced self-assembly for all-solid-state batteries. J Mater Chem A. 2016; 4:8091-8096.

16. T. Sugimoto, "Monodispersed Particles (Second Edition)." Elsevier: Amsterdam, 2019.

17. Y. Wang, D. Lu, M. Bowden, P. Z. El Khoury, K. S. Han, Z. D. Deng, et al. Mechanism of Formation of $Li_7P_3S_{11}$ Solid Electrolytes through Liquid Phase Synthesis. Chem Mater. 2018; 30:990-997.

18. N. H. H. Phuc, T. Yamamoto, H. Muto, and A. Matsuda, et al. Fast synthesis of Li_2S-P_2S_5-LiI solid electrolyte precursors. Inorg Chem Front. 2017; 4:1660-1664.

19. M. Calpa, N. C. Rosero-Navarro, A. Miura, K. Terai, F. Utsuno, et al. Formation Mechanism of Thiophosphate Anions in the Liquid-Phase Synthesis of Sulfide Solid Electrolytes Using Polar Aprotic Solvents. Chem Mater. 2020; 32:9627-9632.

20. Z. Liu, W. Fu, E. A. Payzant, Y. Xiang, C. Liang, et al. Anomalous high ionic conductivity of nanoporous β-Li_3PS_4. J Am Chem Soc. 2013; 135: 975-978.

21. A. Hayashi, S. Hama, T. Minami, M. Tatsumisago, et al. Formation of superionic crystals from mechanically milled Li_2S–P_2S_5 glasses. Electrochem Commun. 2003; 5:111-114.

22. F. Mizuno, A. Hayashi, K. Tadanaga, M. Tatsumisago, et al. High lithium ion conducting glass-ceramics in the system Li_2S–P_2S_5 Solid State Ionics. 2006; 177:2721-2725.

23. S. Teragawa, K. Aso, K. Tadanaga, A. Hayashi, M. Tatsumisago, et al. Liquid-phase

synthesis of a Li_3PS_4 solid electrolyte using N-methylformamide for all-solid-state lithium batteries. J Mater Chem A. 2014; 2:1-2.

24. K. Kaup, L. Zhou, A. Huq, L. F. Nazar, et al. Impact of the Li substructure on the diffusion pathways in alpha and beta Li_3PS_4: an in situ high temperature neutron diffraction study. J Mater Chem A. 2020; 8:12446-12456.

25. M. Calpa, N. C. Rosero-Navarro, A. Miura, K. Tadanaga, et al. Instantaneous preparation of high lithium-ion conducting sulfide solid electrolyte $Li_7P_3S_{11}$ by a liquid phase process. RSC Advances. 2017; 7:46499-46504.

26. N. Machida, H. Yamamoto, S. Asano, T. Shigematsu, et al. Preparation of amorphous $75L_2S \cdot P_2S_3 \cdot (25\text{-}x)P_2S_5$ (mol%) solid electrolytes by a high-energy ball-milling process and their application for an all-solid-state lithium battery. Solid State Ionics. 2005; 176: 473-479.

27. F. M. Delnick, G. Yang, E. C. Self, H. M. Meyer, et al. Investigation of Complex Intermediates in Solvent-Mediated Synthesis of Thiophosphate Solid-State Electrolytes. J Phys Chem C. 2020; 124: 27396-27402.

28. M. Jiang, G. Liu, Q. Zhang, D. Zhou, et al. Ultrasmall Li_2S-Carbon Nanotube Nanocomposites for High-Rate All-Solid-State Lithium-Sulfur Batteries. ACS Appl Mater Interfaces. 2021; 13: 18666-18672.

29. L. Xue, L. Zeng, W. Kang, H. Chen, et al. 3D Printed Li–S Batteries with In Situ Decorated Li_2S/C Cathode: Interface Engineering Induced Loading-Insensitivity for Scaled Areal Performance. Adv Energy Mater. 2021; 11: 2100420.

30. X. Li, C. A. Wolden, C. Ban, Y. Yang, et al. Facile Synthesis of Lithium Sulfide

Nanocrystals for Use in Advanced Rechargeable Batteries. ACS Appl Mater Interfaces. 2015; 7: 28444-28451.

31. M. Duchardt, M. Diels, B. Roling, S. Dehnen, et al. Flow-Oriented Synthesis of Li_2S and Li3PS4·3THF: Opening Up a Completely Solvent-Based Solid Electrolyte Value Chain. ACS Appl Energy Mater. 2020; 3: 6937-6945.

32. B. Fan, H. Fu, H. Li, B. Xue, X. Zhang, Z. Luo, et al. Ionic conductive GeS_2-Ga_2S_3-Li_2S-LiI glass powders prepared by mechanical synthesis. J Alloys Compd. 2018; 740:61-67.

33. S. Ito, M. Nakakita, Y. Aihara, T. Uehara, N. Machida, et al. A synthesis of crystalline $Li_7P_3S_{11}$ solid electrolyte from 1,2-dimethoxyethane solvent. J Power Sources. 2014; 271:342-345.

34. N. H. H. Phuc, M. Totani, K. Morikawa, H. Muto, A. Matsuda, et al. Preparation of Li_3PS_4 solid electrolyte using ethyl acetate as synthetic medium. Solid State Ionics. 2016; 288:240-243.

35. A. Sakuda, A. Hayashi, M. Tatsumisago, et al. Sulfide Solid Electrolyte with Favorable Mechanical Property for All-Solid-State Lithium Battery. Sci Rep. 2013; 3:2261.

36. X. Yang, J. Luo, and X. Sun , et al. Towards high-performance solid-state Li–S batteries: from fundamental understanding to engineering design. Chem Soc Rev 2020; 49:2140-2195.

37. K. Yan, Z. Lu, H.-W. Lee, F. Xiong, P.-C. Hsu, Y. Li, et al. Selective deposition and stable encapsulation of lithium through heterogeneous seeded growth. Nat Energy.

2016; 1:16010.

38. H. Wang, H. Gao, X. Chen, J. Zhu, W. Li, Z. Gong, et al. Linking the Defects to the Formation and Growth of Li Dendrite in All‐Solid‐State Batteries. Adv Energy Mater. 2021; 11:2102148.

39. Y. Zhu, X. He, Y. Mo, et al. Origin of Outstanding Stability in the Lithium Solid Electrolyte Materials: Insights from Thermodynamic Analyses Based on First-Principles Calculations. ACS Appl Mater Interfaces. 2015; 7:23685-23693.

40. W. D. Richards, L. J. Miara, Y. Wang, J. C. Kim, G. Ceder, et al. Interface Stability in Solid-State Batteries. Chem Mater. 2015; 28:266-273.

41. L. Sang, R. T. Haasch, A. A. Gewirth, R. G. Nuzzo, et al. Evolution at the Solid Electrolyte/Gold Electrode Interface during Lithium Deposition and Stripping. Chem Mater. 2017; 29:3029-3037.

42. S. Wenzel, D. A. Weber, T. Leichtweiss, M. R. Busche, J. Sann, et al. Interphase formation and degradation of charge transfer kinetics between a lithium metal anode and highly crystalline $Li_7P_3S_{11}$ solid electrolyte. Solid State Ionics 2016; 286:24-33.

43. U. S. Kasavajjula, C. Wang, P. E. Arce, et al. Discharge Model for $LiFePO_4$ Accounting for the Solid Solution Range. J Electrochem Soc. 2008; 155:A866.

44. X. Yang, Q. Sun, C. Zhao, X. Gao, K. R. Adair, Y. Liu, et al. High-areal-capacity all-solid-state lithium batteries enabled by rational design of fast ion transport channels in vertically-aligned composite polymer electrodes. Nano Energy. 2019; 61:567-575.

45. F. Han, J. Yue, X. Fan, T. Gao, C. Luo, Z. Ma, et al. High-Performance All-Solid-

State Lithium–Sulfur Battery Enabled by a Mixed-Conductive Li_2S Nanocomposite. Nano Lett. 2016; 16:4521-4527.

46. S. Xu, D. W. McOwen, C. Wang, L. Zhang, W. Luo, C. Chen, et al. Three-Dimensional, Solid-State Mixed Electron–Ion Conductive Framework for Lithium Metal Anode. Nano Lett. 2018; 18:3926-3933.